DEFORMATION MODES OF GRADIENT HEXACHIRAL AUXETICS UNDER IMPACT LOADINGS

XIN LI[1] & CHUANQING CHEN[2]
[1]Nanjing University of Science and Technology, Nanjing, China
[2]Nanjing University, Nanjing, China

ABSTRACT
Chiral structures, a special type of negative Poisson's ratio structures, possess excellent energy absorbing capabilities and hold great promise in the field of impact protection. Compared with homogeneous structures, the gradient design of chiral structures can further optimize and enhance their energy absorbing capabilities. In this work, we experimentally and numerically investigated the deformation modes of gradient hexachiral auxetic metamaterials under quasi-static, dynamic and blast loadings. Five gradient design strategies were employed in the test, including uniform (UG), positive (PG), negative (NG), centre positive (CPG), and centre negative gradients (CNG). The effects of gradient distribution on deformation/failure modes under different loading conditions were analysed. Plane impact experimental results revealed that the gradient design can mitigate the shear deformation of hexachiral auxetics, which efficiently remain its negative Poisson's ratio effect under dynamic loading. Compare with the quasi-static loading, earlier failure of auxetics was observed under dynamic loads due to the strain rate and inertial effect, which diluted their negative Poisson's ratio effect and energy absorption capability. Among various gradient designs, the auxetics with negative gradient configurations exhibit the best energy absorption capability under dynamic loadings. Under blast loads, the various gradient types of auxetic cores exhibited distinct compression deformation behaviours. The hexachiral cores in sandwich panels with larger radius nodes on the blast surface are more likely to undergo compression deformation. The NG and CNG cores, featuring nodes resistant to flattening deformation, are more effective in generating NPR effect, resulting in a larger impact resistance. In addition, by using finite element method, the deformation mods of gradient hexachiral auxetics are further investigated under higher impact velocities and blast loadings to reveal loading rate effects on their deformation modes. This work offers profound insights into enhanced performance mechanisms and provides avenues for optimizing structural design of auxetic metamaterials.
Keywords: hexachiral, gradient, impact and blast loadings, deformation mode.

1 INTRODUCTION

Chiral structures, a unique class of auxetic mechanical metamaterials, are characterized by their negative Poisson's ratio (NPR) behaviour, which manifests as transverse expansion under longitudinal compression or shrinkage under tension [1]. This distinctive deformation pattern arises from their microstructural architecture rather than the intrinsic properties of the constituent materials. As a result, chiral structures exhibit a range of advantageous mechanical properties, including enhanced fracture resistance, superior shear resistance, improved indentation resistance, and exceptional energy absorption capabilities [2], [3]. These attributes make chiral structures highly promising for applications in impact protection, blast mitigation, and energy dissipation during extreme loading events [4], [5].

Hexachiral structures, first proposed by Prall and Lakes [6], exhibit an in-plane Poisson's ratio of −1, which has been both theoretically and experimentally validated. This unique behaviour, characterized by full-wave-shaped ligament deformation under loading, contributes to their superior energy absorption capabilities compared to other chiral configurations, such as anti-chiral structures, which exhibit half-wave-shaped deformation [7].

WIT Transactions on The Built Environment, Vol 215, © 2025 WIT Press
www.witpress.com, ISSN 1743-3509 (on-line)
doi:10.2495/SUSI250181

Recent advancements in chiral structure design have further diversified their applications [8]. In addition to traditional two-dimensional (2D) chiral structures, three-dimensional (3D) chiral configurations [9]–[12] have been developed, offering enhanced mechanical properties and dynamic performance. Moreover, the introduction of gradient design strategies has opened new avenues for optimizing the mechanical behaviour of chiral structures [13]–[15]. Gradient designs, which involve the integration of sub-structures with varying characteristics, such as cell wall thickness, material composition, or geometric parameters, have been shown to improve stiffness, strength, and energy absorption capabilities [16], [17]. These functionally graded auxetic structures exhibit superior performance under dynamic loading conditions, making them ideal for applications requiring impact resistance and energy dissipation.

Despite the growing interest in chiral structures, particularly in the context of gradient designs, there remains a significant research gap in understanding their deformation mechanisms and energy absorption capabilities under different loading conditions. Most existing studies have focused on uniform structures or have been limited to numerical simulations, often neglecting the effects of material damage and strain rate sensitivity. Furthermore, while gradient designs have shown promise in enhancing mechanical properties, their performance under extreme loading conditions, such as high-velocity and blast impacts, has not been thoroughly investigated.

In this work, based on our previous studies [14], [15], we address these gaps by conducting a comprehensive experimental and numerical investigation into the mechanical responses of gradient hexachiral auxetic metamaterials under quasi-static, impact, and blast loadings. Five distinct gradient design strategies – uniform (UG), positive (PG), negative (NG), centre positive (CPG), and centre negative (CNG) gradients – were employed to fabricate hexachiral structures using 3D printing technology. The deformation modes and Poisson's ratio effects of these structures were evaluated under plane compression conditions with various impact velocities. The deformation process and final deformation modes of these structures, when used as cores in sandwich panels under blast loads, were also studied. Additionally, based on the validated finite element (FE) models, we performed numerical analyses for higher impact velocities and more intense explosive loads.

2 GRADIENT AUXETIC CONFIGURATIONS

The hexachiral [6] configuration unit consists of six ligaments, each with a length denoted as L, and these are connected tangentially to a circular node with an outer radius of r, as illustrated in Fig. 1. The wall thicknesses of the node and the ligament are defined as t_n and t_l, respectively. The overall height of the structure is H. In this work, based on the uniform gradient (UG) configuration, an in-depth elucidation of the design methodologies for gradient hexachiral auxetics will be presented, encompassing positive gradient (PG), negative gradient (NG), centre positive gradient (CPG), and centre negative gradient (CNG). The gradient design principle is based on the ratio of node radii between adjacent layers, which are delineated by dashed lines and labelled as $n+1$, n and $n-1$ from top to bottom. The radii of these layers are denoted as r_{n+1}, r_n and r_{n-1}, with R representing the distance between node centres in adjacent layers. To quantify the gradient, a gradient factor ω is introduced [14], [15], defined as the ratio of node radii between upper and lower adjacent layers:

$$\omega = r_n / r_{n-1}. \tag{1}$$

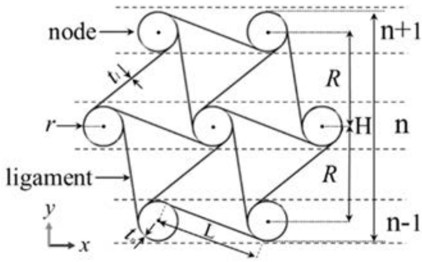

Figure 1: Geometric parameters of hexachiral auxetic cell structure [14].

The UG design is characterized by ω equal to 1, indicating uniform node radii throughout the structure. The PG design features ω greater than 1, with node radii decreasing from top to bottom. In contrast, the NG design has ω less than 1, with increasing radii values. The CPG and CNG designs are variations of the PG and NG configurations, respectively, with node radii exhibiting rotational symmetry around the structure's central point, leading to reciprocal gradient factors between the upper and lower sections. For CPG and CNG, the gradient factor above the central axis is considered the representative value.

3 EXPERIMENTAL PROCEDURE

3.1 Quasi-static and dynamic loadings

In this section, quasi-static and dynamic compression tests are conducted under plane compression velocities of 10 mm/min and 5 m/s for analysing the deformation modes of gradient hexachiral auxetics. To enhance the capture of detailed deformation characteristics during compression, the auxetics were designed with 5 node layers, as illustrated in Fig. 2. Arrows indicate the progression from larger to smaller node radii. The UG configuration served as the baseline, with specific parameters set as follows: r = 4.8 mm, t_l = t_n = 1.22 mm, L/r = 3.65 and H = 73 mm. For the PG, NG, CPG, and CNG configurations, their respective ω values were set to be 1.1, 0.91, 1.1, 0.91, respectively. The cell wall thicknesses for PG, NG, CPG, and CNG were determined to be 1.22, 1.22, 1.20, and 1.26 mm, respectively. Detailed specimen information and experimental methods can be found in Chen et al. [14].

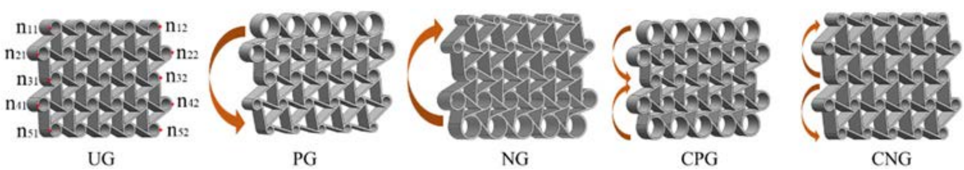

Figure 2: Different gradient types of hexachiral structures for plane compression test.

Fig. 3 depicts the deformation profiles of gradient hexachiral auxetics at vertical strains (ε_y) ranging from 0.1 to 0.6 under quasi-static load. At ε_y= 0.1, the deformation is localized mainly to the central node layer, where node rotation and ligament bending cause contraction. This inward shrinkage is the primary contributor to the NPR effect observed at this stage.

Deformation amplitudes differ across configurations, with UG and CNG showing the most significant changes, followed by PG and NG, and CPG exhibiting the least deformation. Larger node radii, which increase curvature, reduce bending stiffness, promoting node flattening in PG, NG, and CPG configurations. This results in shorter effective compression distances at the same strain, reducing rotational deformation in these designs. At the ε_y of 0.2 and 0.3, a more pronounced global NPR effect is observed, primarily due to the horizontal contraction caused by the rotational deformation of nodes in layers beyond the central one. The voids between the ligaments and nodes are crucial in facilitating the NPR effect in hexachiral auxetics. At ε_y of 0.4, these voids have largely disappeared, with compression occurring within the nodes themselves. Detailed observation indicates that all specimens' horizontal deformation at a strain of 0.5 exceeds that at 0.4, indicating a reduction in the NPR effect's intensity. At around a compressive strain of 0.6, the voids within the circular nodes are nearly completely compressed, leading to a fully densified structure.

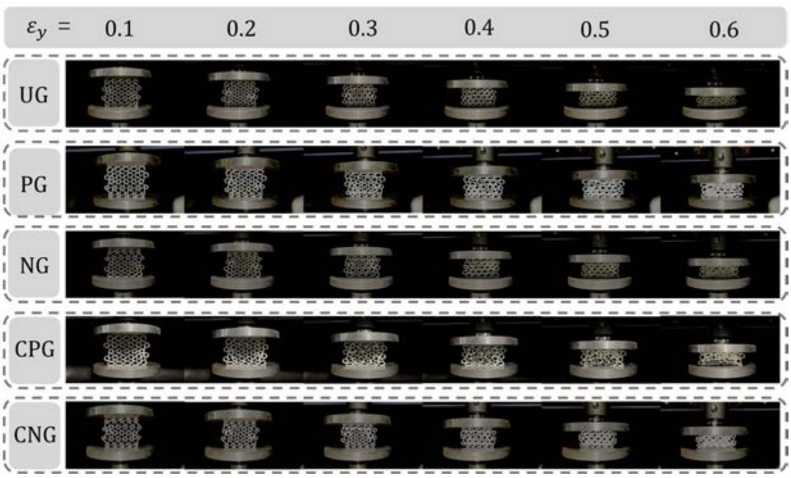

Figure 3: Deformation modes of diverse gradient hexachiral auxetics under quasi-static loading [14].

In addition, the Poisson's ratio υ of auxetics is defined as a negative ratio of the average horizontal strains of each layer to the vertical strain. At the vertical strain range 0.1–0.5, it can be written as

$$\upsilon = \sum_{i=1}^{5} {\varepsilon_x}^i / (5\varepsilon_y), \tag{2}$$

where ${\varepsilon_x}^i$ is the horizontal strain of ith node layer, which can be calculated by the ratio of the changing horizontal width of each node layer at varying compression levels to its initial width. The width of each node layer is ascertained by measuring the distance between the centre points of the side nodes at the layer's edges, marked by dots of UG in Fig. 2.

The quasi-static Poisson's ratio of different gradient hexachiral auxetics are listed in Table 1. A more negative value signifies a more pronounced NPR effect. Overall, the CNG configuration exhibits the most pronounced NPR effect, while the CPG configuration demonstrates the least. And the NPR effect in PG and NG is quite similar, slightly inferior to that of UG.

Table 1: Poisson's ratio values of gradient hexachiral auxetics under quasi-static load.

Gradient	Strain					
	0.1	0.2	0.3	0.4	0.5	0.6
UG	−0.40	−0.54	−0.53	−0.37	−0.22	−0.02
PG	−0.32	−0.49	−0.46	−0.32	−0.20	−0.05
NG	−0.35	−0.47	−0.39	−0.29	−0.16	−0.06
CPG	−0.08	−0.15	−0.12	−0.07	−0.04	0
CNG	−0.68	−0.58	−0.52	−0.43	−0.29	−0.04

Fig. 4 presents the deformation profiles of various gradient hexachiral auxetics at ε_y ranging from 0.1 to 0.6, subjected to an impact velocity of 5 m/s. At ε_y of 0.1, the deformation modes are similar to those under quasi-static loading (Fig. 3), with node rotation in the central layer and flattening of large-radius nodes. However, dynamic loading introduces inertial effects and stress wave propagation, leading to localized stress concentration and additional stress on the structure. As a result, structural damage occurs at lower strains (ε_y = 0.2), causing significant changes in the deformation modes compared to quasi-static conditions. Particularly in the UG configuration, shear deformation along the diagonal is observed, caused by the quasi-parallelogram distribution of nodes during auxetic deformation, allowing shear force transmission. Other configurations do not show shear deformation, despite experiencing local damage. This is likely due to their distinct node radius distributions, which form a quasi-trapezoidal structure, enhancing stability and reducing shear deformation. Localized damage in hexachiral auxetics weakens the NPR

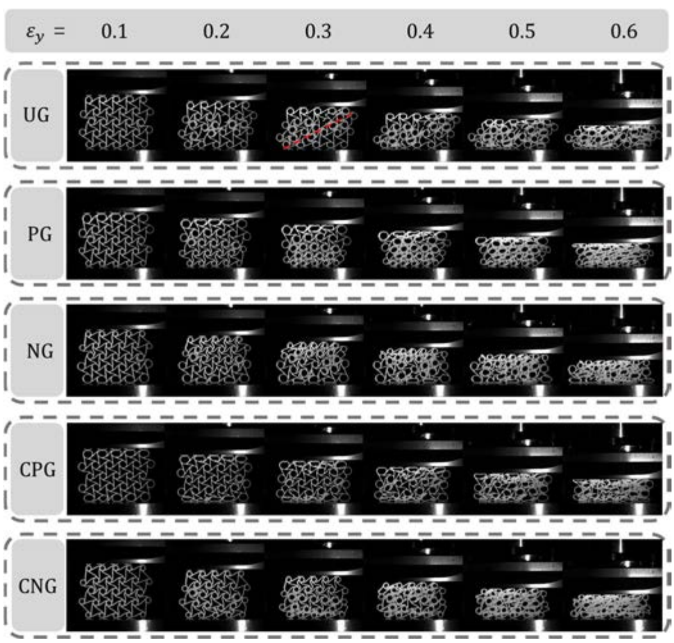

Figure 4: Deformation modes of diverse gradient hexachiral auxetics under dynamic loading [14].

effect, particularly in the UG configuration, where shear deformation splits the structure into two parts, deforming in opposite directions.

Table 2 presents the Poisson's ratio of different gradient hexachiral auxetics under dynamic compression. The NPR effect of the CNG configuration is comparable to that of the PG configuration, followed by the NG configuration, while the UG and CPG configurations exhibit the weakest NPR effect. In addition, through detailed numerical comparisons with quasi-static condition, the overall Poisson's ratio curves for UG, NG and CNG experience increases, signifying a weakening of the NPR effect under v = 5 m/s in these three configurations. It can be attributed to occurrence of the localized structure damage caused by inertial effects and wave propagation.

Table 2: Poisson's ratio values of gradient hexachiral auxetics under 5 m/s.

Gradient	Strain					
	0.1	0.2	0.3	0.4	0.5	0.6
UG	−0.55	−0.17	−0.05	0.07	0.11	0.24
PG	−0.32	−0.46	−0.48	−0.34	−0.20	0.24
NG	−0.34	−0.40	−0.32	−0.17	−0.05	0.10
CPG	−0.13	−0.16	−0.11	−0.06	0.02	0.03
CNG	−0.63	−0.48	−0.42	−0.28	−0.16	0.04

3.2 Blast loading

The compression modes of hexachiral auxetic cores under explosion load were investigated, with Fig. 5 illustrating the geometry and dimensions of the sandwich panel specimen and their gradient hexachiral cores. The face sheets, attached to both sides of the core, had a length (L) and width (W) of 300 mm and a typical thickness of 0.4 mm. The cores featured hexachiral structures of various gradient types with three node layers. These cores had a fixed height (H) of 21 mm, which is a common size used in practical engineering. The UG configuration was chosen as a reference standard, with the following parameters: the outer radius (r) of the hexachiral nodes was 2.4 mm, and both the ligaments (t_l) and nodes (t_n) had a thickness of 0.838 mm. For the PG, NG, CPG, and CNG configurations, ω values were set to 1.25, 0.8, 1.25, and 0.8, respectively. Correspondingly, the cell wall thicknesses (t) were 0.840, 0.840, 0.822, and 0.854 mm, respectively. Detailed specimen information and experimental methods can be found in Chen et al. [15].

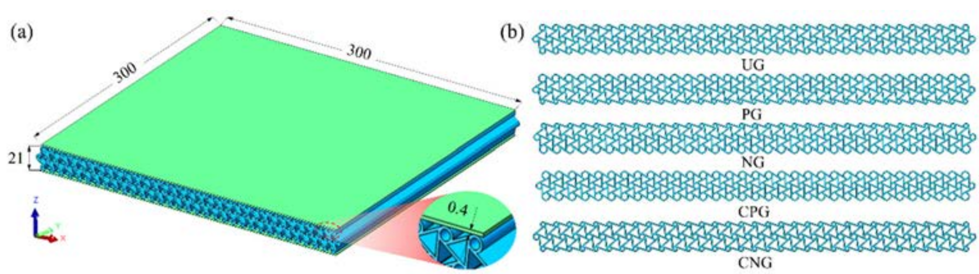

Figure 5: (a) The 3D structure of auxetic core sandwich panel [15]; and (b) Different gradient types of hexachiral cores for explosion test.

Fig. 6 shows the central cross-sections of five gradient hexachiral core specimens subjected to blast loads equivalent to 42 g of TNT. The specimens were exposed to impulses of 31.29, 36.90, 30.45, 28.02, and 37.80 Ns measured in blast experiment. Deformation was concentrated in three main areas: the central region (highlighted by red dotted rectangles) and the clamped regions on both sides (marked by red solid lines). The clamped areas deformed primarily due to the constraining effect of the steel frame, limiting the specimen's movement. In contrast, the central region experienced the most significant deformation, as it was directly affected by the blast load. The NPR effect was assessed by observing node rotation and ligament bending around them. Except for the PG configuration, all cores experienced deformation confined to the first ligament layer, restricting the NPR effect. The UG-3 and CPG-3 specimens exhibited similar compressive deformation, with node flattening near the front face sheet and bending in the first ligament layer. Little plastic deformation was observed in the deeper layers, and despite a smaller impulse, CPG-3 showed more node flattening than UG-3. NG-3, with an impulse similar to UG-3, demonstrated superior compression resistance, with minimal node deformation and slight bending in the first ligament layer, much less than UG-3. PG-3 experienced the most deformation, including extensive flattening and bending in both the first and second layers of nodes and ligaments, along with multiple joint fractures, due to a higher impulse. In contrast, CNG-3, subjected to a similar impulse as PG-3, showed less deformation, with bending primarily in the first ligament layer and fewer joint fractures. The findings indicate that node size significantly influences blast compression deformation. Configurations with larger nodes adjacent to the front face sheet, such as PG and CPG, were more prone to compression deformation. Conversely, configurations with smaller nodes, such as NG and CNG, were less susceptible to compression deformation. This is because larger nodes have a greater curvature radius, leading to lower bending stiffness, making larger-radius nodes more prone to deformation under external forces.

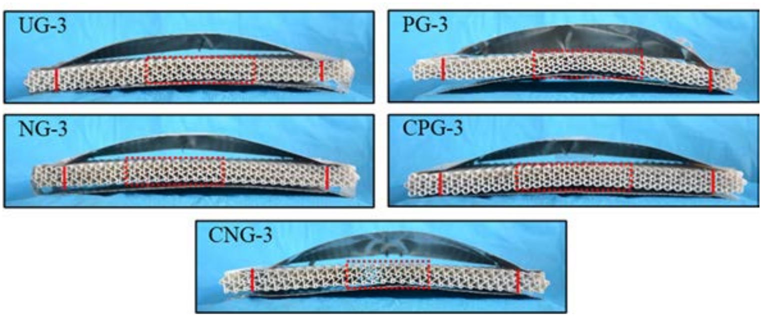

Figure 6: Compression deformation of specimens with different gradient auxetic cores [15].

4 SIMULATIONS

To gain deeper insights into the deformation mechanisms of gradient hexachiral auxetic structures and their compressive behaviour under higher impact velocity and blast loading, FE simulations were performed. Prior studies established validated FE models for plane compression using Abaqus [14] and for blast loading using LS-DYNA [15]. Building on these validated frameworks, simulations were conducted under planar compression at 20 m/s and 50 m/s, as well as blast loads equivalent to 70 g and 100 g TNT, to analyse the deformation modes of gradient hexachiral auxetics under extreme dynamic conditions. One noteworthy aspect of the simulations was the approach to material failure: it was considered in the planar compression simulations but excluded from the blast loading simulations. This decision was rooted in experimental observations showing that significant structural damage occurred during planar compression tests, while blast loading led to damage mainly seen as tearing between printed layers, with minimal in-plane structural damage. Two key reasons were identified for this phenomenon: (1) The wall thickness to node radius (or ligament length) of the specimens tested under blast loading was relatively large, leading to high stiffness, which made them less prone to in-plane structural damage. (2) Applied blast loading is a localized type of load, which more easily causes shear or tensile tearing between layers when subjected to a 3D printed plate. Here, we primarily focus on in-plane compression modes.

4.1 FE results

4.1.1 Impact loading

Numerical simulations of gradient hexachiral structures subjected to high-velocity planar compression revealed distinct deformation patterns. Figs 7 and 8 depict the structural response at compressive strains ranging from 0.1 to 0.5 under impact velocities of 20 m/s and 50 m/s, respectively. At 20 m/s, damage initiation occurred at significantly smaller strains (< 0.1) compared to lower-impact scenarios as shown in Figs 3 and 4, accompanied by a pronounced deformation gradient across the structure – a phenomenon attributed to the micro-inertial effect. This effect highlights how dynamic loading accelerates localized deformation and stress redistribution. The geometry of nodal regions played a critical role in governing structural integrity. Structures with larger node radii near the impactor (e.g., UG, PG, CPG) exhibited severe damage, whereas designs with smaller radii (e.g., NG, CNG) demonstrated reduced nodal failure. This underscores the sensitivity of hexachiral auxetics to node geometry, as their energy dissipation primarily relies on node rotation and ligament bending. Node damage may disrupt the quasi-static constitutive relationships, altering failure modes and energy absorption mechanisms, which ultimately impacts macroscopic mechanical performance. A key observation was the influence of gradient design of hexachiral structures on deformation uniformity. The NG structure, characterized by a stiffness gradient decreasing from top to bottom, achieved more homogeneous deformation. The stiffer upper region absorbed the majority of the impact energy, while the compliant lower region accommodated deformation, mitigating stress concentration and delaying structural collapse. In contrast, the CNG structure, despite sharing identical stiffness near impactor region with NG, suffered severe localized damage due to its uniformly high stiffness in the lower region. This rigidity restricted structure deformation and energy dissipation, leading to stress accumulation and premature failure near the impactor.

Under a high-velocity impact of 50 m/s, all gradient hexachiral structures exhibit a distinct layered ‘I’-shaped deformation mode that propagates sequentially from the impact end to the fixed end (Fig. 8). This deformation behaviour arises from the synergistic interaction between inertial effects and stress wave propagation. At the impact end, localized inertial resistance causes rapid stress accumulation, forming a crushed zone (evident at a strain of 0.1), while the delayed arrival of stress waves temporarily preserves the undeformed state in distal regions, dynamically separating the structure into a ‘crushed zone’ and a ‘delayed deformation zone’. It can be anticipated that further increasing the impact velocity would narrow the gap between the stress wave propagation speed and the impact velocity, dividing the structure into crushed and delayed deformation zones at the shock front. Under such

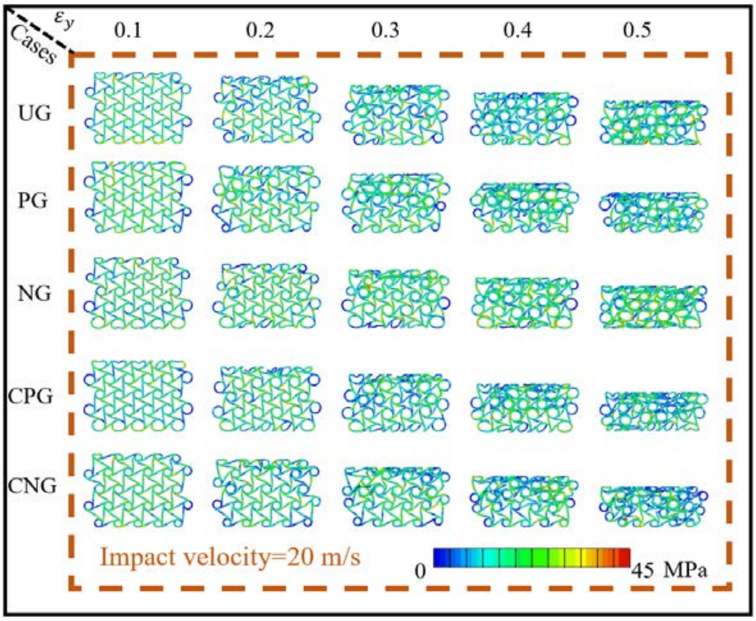

Figure 7: Compression deformation of specimens with different gradient auxetic cores under impact velocity of 20 m/s.

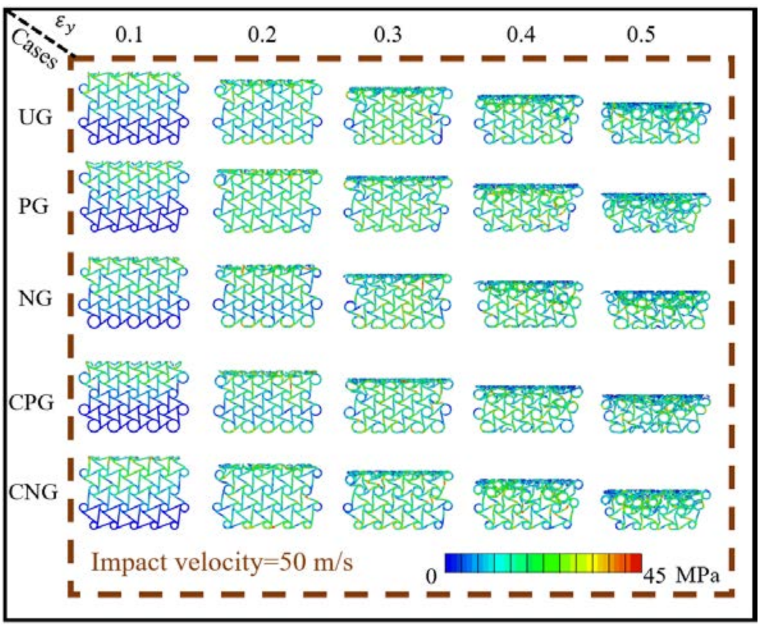

Figure 8: Compression deformation of specimens with different gradient auxetic cores under impact velocity of 50 m/s.

conditions, the crushed zone experiences significantly higher stress concentrations, with a discontinuous stress and deformation behaviour across the whole structure.

4.1.2 Blast loading

This section investigates the dynamic response of hexachiral core sandwich panels under 70 g and 100 g TNT blast loads using validated FE models. The deformation processes and final modes are illustrated in Figs 9 and 10. The deformation processes of PG specimen under 100 g TNT blast load are illustrated in Fig. 9. The blast shockwave, propagating as compressive waves, initially impacts the front face sheet, inducing transient deformation (Fig. 9(a)). Subsequently, interfacial separation occurs between the front face sheet and the core due to their divergent deformation rates (Fig. 9(b)). During this phase, the core and the back-face sheet remain coupled, moving synchronously to the maximum displacement position without significant separation (Fig. 9(c)). Afterward, the core and the back panel rebound together. In the rebound stage, the rebound amplitudes of these two components are smaller compared to the maximum compression displacement and the compressed core retaining permanent plastic deformation. This is in contrast to the larger rebound observed under smaller blast loads, as reported in previous literature, mainly due to the more significant plastic deformation under larger blast loads. Notably, complete separation between the core and back face sheet emerges during rebound due to rebound velocity mismatch (Fig. 9(d)). Ultimately, the structure stabilizes in a residual deformation state through damping oscillations.

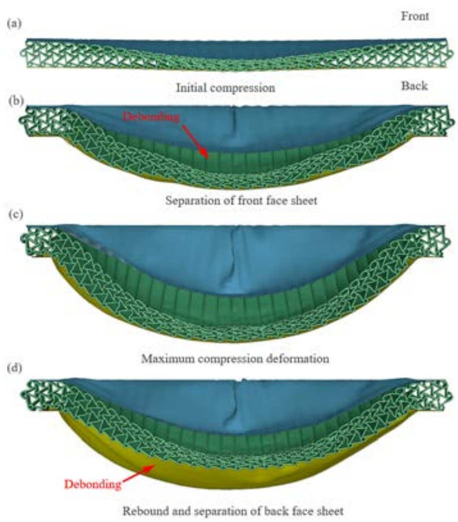

Figure 9: Cross section profiles of deformation progress under blast load (100 g TNT) of PG specimen.

Fig. 10 provides the final deformation modes of different gradient hexachiral cores under 70 g (represented by '1') and 100 g (represented by '2') TNT blast loads. The frontal (δ_1) and back (δ_2) displacements of core are measured, and then the core compression amounts $\Delta\delta$ can be calculated as $\delta_1 - \delta_2$. Under 70 g TNT blast load, The CPG core exhibits the largest compression ($\Delta\delta$ = 9.29 mm), followed by UG (8.70 mm), PG (8.10 mm), NG

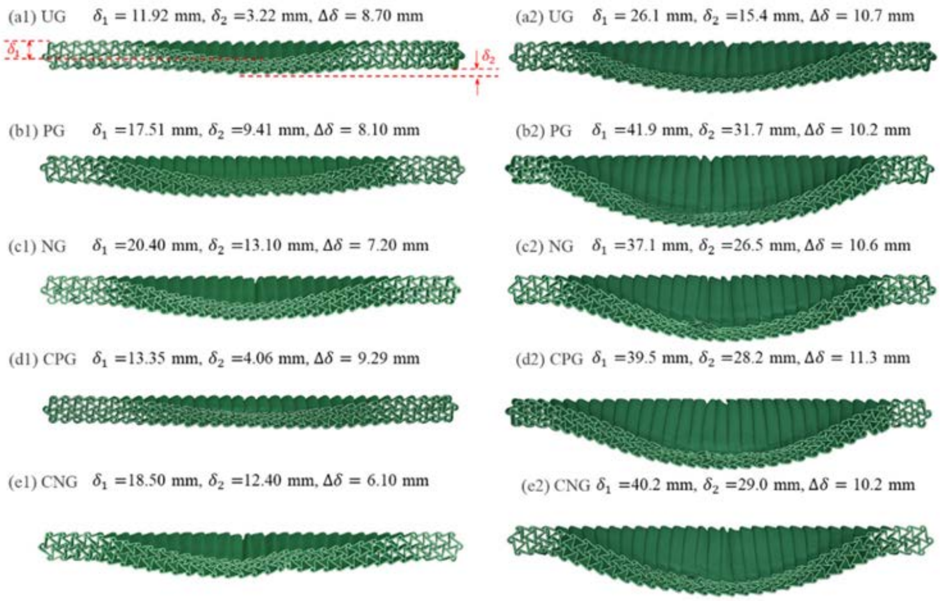

Figure 10: Compress deformation of cores with different gradient strategies: (1) 70 g [15]; and (2) 100g TNT blast loads.

(7.20 mm), and CNG (6.10 mm). While UG, PG, and CPG cores undergo greater compression, their deformation is dominated by first-layer node flattening, which undermines the rigid-node assumption critical for achieving the NPR effect in chiral auxetics. This flattening restricts NPR behaviour by limiting node rotation and ligament bending – key mechanisms for auxetic. Conversely, NG and CNG cores, with smaller node compression, preserve nodal rigidity, enabling pronounced NPR deformation through coordinated node rotation and ligament bending. The enhanced NPR effect in NG and CNG cores correlates with higher structural stiffness.

Under the 100 g TNT blast load, the compression and compressed regions of the cores increased compared to the 70 g TNT load. However, the compression amounts ($\Delta\delta$) across the different gradient hexachiral cores did not exhibit significant differentiation. The CPG core having the highest compression ($\Delta\delta$ = 11.3 mm), while the compression values for the other structures fell within the range of 10.2 to 10.7 mm. This is primarily due to the larger blast load causing plastic compression behaviour across the entire node layers of the core. Notably, the gradient cores exhibited significantly larger plastic deformation regions compared to the UG structure, which has a uniform node distribution. This difference is reflected in the δ_1 values: UG has δ_1 = 26.1 mm, while the largest value, observed in PG, is δ_1 = 41.9 mm, showing a 41.3% difference. A larger plastic deformation area may imply greater energy dissipation, which ultimately enhances the protective performance of the structure.

5 CONCLUSION

Gradient strategies play significant roles in the deformation modes of hexachiral auxetics under different loading conditions. Dynamic loading introduces earlier and more structural damage than quasi-static conditions, reducing NPR effects. Gradient design can mitigate the shear deformation under dynamic loadings. In both quasi-static and dynamic loading conditions, the CNG configuration exhibits a substantial NPR effect, while the CPG configuration performs the least. Under blast loads, configurations with larger nodes adjacent to the front face sheet are more prone to compression deformation. Numerical results show that at a 20 m/s impact velocity, the NG gradient design promotes more uniform deformation across the structure, while other designs exhibit a gradient deformation pattern. Under higher impact loads (50 m/s), all structures exhibit a sequential 'I'-shaped collapse mode driven by inertial effects and stress wave propagation. Similarly, under a larger 100 g TNT blast load, the cores experience more severe compression, with PG, NG, CPG, and CNG showing larger plastic deformation regions.

ACKNOWLEDGEMENT

This work was supported by the National Natural Science Foundation of China (Grant No. 12172164).

REFERENCES

[1] Evans, K.E., Nkansah, M.A., Hutchinson, I.J. & Rogers, S.C., Molecular network design. *Nature*, **353**, p. 124, 1991. https://doi.org/10.1038/353124a0.

[2] Chen, C., Airoldi, A., Caporale, A.M., Sala, G. & Yin, X., Impact response of composite energy absorbers based on foam-filled metallic and polymeric auxetic frames. *Composite Structures*, **331**, 117916, 2024. https://doi.org/10.1016/j.compstruct.2024.117916.

[3] Airoldi, A., Novak, N., Sgobba, F., Gilardelli, A. & Borovinšek, M., Foam-filled energy absorbers with auxetic behaviour for localized impacts. *Materials Science and Engineering: A*, **788**, 139500, 2020. https://doi.org/10.1016/j.msea.2020.139500.

[4] Linforth, S.J., Auxetic armour system for protection against soil blast loading. The University of Melbourne, 2020.

[5] Imbalzano, G., Tran, P., Ngo, T.D. & Lee, P.V., Three-dimensional modelling of auxetic sandwich panels for localised impact resistance. *Journal of Sandwich Structures and Materials*, **19**, pp. 291–316, 2017. https://doi.org/10.1177/1099636215618539.

[6] Prall, D. & Lakes, R.S., Properties of a chiral honeycomb with a Poisson's ratio of −1. *International Journal of Mechanical Sciences*, **39**, pp. 305–314, 1997. https://doi.org/10.1016/S0020-7403(96)00025-2.

[7] Alderson, A. et al., Elastic constants of 3-, 4- and 6-connected chiral and anti-chiral honeycombs subject to uniaxial in-plane loading. *Composites Science and Technology*, **70**, pp. 1042–1048, 2010. https://doi.org/10.1016/j.compscitech.2009.07.009.

[8] Wu, W., Hu, W., Qian, G., Liao, H., Xu, X. & Berto, F., Mechanical design and multifunctional applications of chiral mechanical metamaterials: A review. *Materials and Design*, **180**, 107950, 2019. https://doi.org/10.1016/j.matdes.2019.107950.

[9] Caporale, A.M., Airoldi, A. & Novak, N., A novel body centered cubic 3D auxetic chiral geometry. *Smart Mater. Struct.*, **34**, 015050, 2024. https://doi.org/10.1088/1361-665X/ad9dc9.

[10] Jiang, Y. & Li, Y., Novel 3D-printed hybrid auxetic mechanical metamaterial with chirality-induced sequential cell opening mechanisms. *Advanced Engineering Materials*, **20**, 1700744, 2018. https://doi.org/10.1002/adem.201700744.

[11] Fu, M., Liu, F. & Hu, L., A novel category of 3D chiral material with negative Poisson's ratio. *Composites Science and Technology*, **160**, pp. 111–118, 2018. https://doi.org/10.1016/j.compscitech.2018.03.017.

[12] Frenzel, T., Kadic, M. & Wegener, M., Three-dimensional mechanical metamaterials with a twist. *Science*, **358**, pp. 1072–1074, 2017. https://doi.org/10.1126/science.aao4640.

[13] Sadikbasha, S. & Pandurangan, V., Crashworthiness of auxetic hexachiral core under in-plane loading. *Materials Today: Proceedings*, 2023. https://doi.org/10.1016/j.matpr.2023.02.267.

[14] Chen, C. et al., Quasi-static and dynamic responses of gradient hexachiral auxetics: Experimental and numerical analysis. *Materials Today Communications*, **41**, 110670, 2024. https://doi.org/10.1016/j.mtcomm.2024.110670.

[15] Chen, C., He, Y., Xu, R., Gao, C., Li, X. & Lu, M., Dynamic behaviors of sandwich panels with 3D-printed gradient auxetic cores subjected to blast load. *International Journal of Impact Engineering*, **188**, 104943, 2024. https://doi.org/10.1016/j.ijimpeng.2024.104943.

[16] Qi, D., Lu, Q., He, C., Li, Y., Wu, W. & Xiao, D., Impact energy absorption of functionally graded chiral honeycomb structures. *Extreme Mechanics Letters*, **32**, 100568, 2019. https://doi.org/10.1016/j.eml.2019.100568.

[17] Qi, C., Jiang, F. & Yang, S., Advanced honeycomb designs for improving mechanical properties: A review. *Composites Part B: Engineering*, **227**, 109393, 2021. https://doi.org/10.1016/j.compositesb.2021.109393.